Effects of single- and multi-stage solid solution treatments on microstructure and properties of as-extruded AA7055 helical profile

Cun-sheng ZHANG, Zhao-gang ZHANG, Ming-fu LIU, En-cheng BAO, Liang CHEN, Guo-qun ZHAO

Key Laboratory for Liquid−Solid Structural Evolution & Processing of Materials (Ministry of Education),
Shandong University, Ji'nan 250061, China

Abstract: The effects of single-stage solution treatment (SST), enhanced solution treatment (EST), high-temperature pre-precipitation (HTPP) and multi-stage solution treatment (MST) on the microstructure, mechanical properties and corrosion resistance of the as-extruded 7055 aluminium alloy (AA7055) helical profile were investigated using differential scanning calorimetry (DSC), optical microscopy (OM), scanning electron microscopy (SEM), electron back-scattered diffraction (EBSD) and transmission electron microscopy (TEM). It was observed that EST and MST could promote the dissolution of the second-phase particles compared with the traditional SST, and the intergranular phases were distinctly discontinuously distributed after HTPP and MST. There was obvious difference in the main texture type and texture strength for the alloy after different solid solution treatments. HTPP could improve the corrosion resistance of the alloy by regulating the intergranular phases, but the mechanical properties were severely weakened. While the good corrosion resistance of the alloy could be obtained by MST without obvious strength loss. As a result, the MST is an ideal solid solution treatment scheme for AA7055.

Key words: 7055 aluminum alloy; extruded profile; solid solution treatment; mechanical properties; corrosion resistance

1 Introduction

Al−Zn−Mg−Cu alloys (7xxx aluminum alloys) are widely used in aeronautic and aerospace engineering due to their high specific strength, low density and good heat treatment performance [1,2]. The hot extrusion technology is an effective forming means for Al−Zn−Mg−Cu alloys [3−5]. During the hot extrusion process of the aluminum alloys, various kinds of precipitated phases form and affect the microstructure and mechanical properties of the alloy. For the typical 7055 aluminum alloys, the high contents of Mg and Zn in the alloy cause the formation of various insoluble eutectic phases, and coarse crystalline phases could easily result in the stress concentration and crack initiation of the alloy [6−8]. In addition, there is a high volume fraction of aging strengthening phases and the precipitated phases largely cover the grain boundaries (GBs) in the alloy. Therefore, by determining the proper solid solution process to optimize the morphology, size and distribution of precipitated phases, a good combination of mechanical properties and corrosion resistance of the alloy could be obtained [9−11].

The purpose of the solid solution treatment is to make the alloying elements dissolve into the Al matrix and to obtain the supersaturated solid solutions by quenching, so as to achieve an excellent strengthening effect in the subsequent aging precipitation stage [12]. Single-stage solution treatment (SST) is a commonly used solid solution method, where the single and constant temperature

is used by only changing the holding time during the solution process [13]. WANG et al [12] revealed the evolution of the Fe-rich phase particles and recrystallization texture with solution time. HAN et al [13] found that the residual phases in AA7050 could be re-dissolved into the Al matrix as the temperature increased, while the volume fraction of recrystallized grains and the sub-grain size would increase accordingly. PENG et al [14] found that the evolution of the second phases of Al−Zn−Mg−Cu alloy during the SST heating process could be divided into three stages: the precipitation of $MgZn_2$ phase at low temperature, the dissolution of the $MgZn_2$ phase and the coarsening of the Al_2CuMg phase at medium temperature and the dissolution of the Al_2CuMg phase at high temperature. DIMAS and BONDAN [15] found that the rational increase of solution temperature could improve the hardness of extruded profile after aging, but the transition liquid phase must be avoided during the solution process. Therefore, the SST temperature must be limited to less than the polyphase eutectic point, and it is hard to dissolve the residual phases completely.

Enhanced solution treatment (EST) performs two-stage heating and temperature-holding process to improve solid solubility and prevent overburning (the first stage holding temperature is lower than the non-equilibrium eutectic temperature, while that of the second stage is higher) [16−18]. SONG and CHEN [16] found that the width of continuously distributed precipitates at the GBs decreased, while the continuous grain boundary precipitates (GBPs) transformed into the discontinuous precipitate structures after EST. SOKOLOWSKI et al [19] found that the Cu-rich phase after EST was effectively refined, and the strength was significantly improved, compared with the conventional SST. CHEN et al [20] compared different EST schemes for AA7055 extruded bar, and the maximum tensile strength of 805 MPa and fracture toughness of 41.5 MPa·m$^{1/2}$ were obtained by a reasonable EST scheme. KONGIANG et al [21] found that EST reduced the formation of coarse black particles while maintaining the same dissolution of eutectic $MgZn_2$ phase similar to SST. PENG et al [22] revealed that the reasonable second-stage solution temperature could improve the stress corrosion resistance. But the degree of recrystallization would be greatly increased at a high solution temperature, and finally the stress corrosion resistance would be weakened.

High temperature pre-precipitation (HTPP) was carried out by holding the alloy at a lightly reduced temperature after EST [23−25]. CHEN and HUANG [23] observed that the intergranular precipitates of AA7055 after HTPP were limited at the GBs, which enhanced the discontinuity of the precipitated phases in the subsequent aging process, and consequently the stress corrosion resistance was improved. HUANG et al [24] concluded that high Cu content in the equilibrium phases of the GBs could reduce the potential difference between the GBPs and Al matrix, resulting in a slow dissolution rate of the anode and eventually lowering the sensitivity to corrosion. LI et al [25] considered that the roughening discontinuous effect of GBPs was more obvious at a decreasing pre-precipitation temperature.

During multi-stage solution treatment (MST), the heating and holding processes are divided into several stages from low temperature to high temperature [26]. DENG et al [26] observed that the texture of the hot-rolled AA7050 sheet was not sensitive to the MST process, but the orientation density decreased as the solution temperature increased, and the change of microstructure and texture mainly depended on the recovery and dynamic recrystallization. XU et al [27] found that the η phase ($MgZn_2$) particles in AA7150 were completely dissolved at 475 °C for 5 min, while the heating temperature should be up to 495 °C to dissolve S phase (Al_2MgCu) particles, and the recrystallization rate could be controlled below 50%. YANG et al [28] considered that the corrosion resistance and fracture toughness of Al−Zn−Mg−Cu alloy were greatly affected by the sharp angles and edges of residual large particles. A feasible MST scheme for spheroidizing process was proposed to achieve the improvement of the strength and corrosion resistance.

From the above analysis, the attention on the solid solution treatment of aluminum alloys (especially 7xxx aluminum alloys) has been mostly focused on the traditional SST and EST for the as-cast alloy or rolled sheets. Therefore, the purpose of this work is to investigate and compare the effects of different solution systems (SST, EST, HTPP, MST) on the microstructures (second-phase distribution, grain orientation, texture distribution,

etc.), the mechanical properties (hardness, strength and ductility), and the corrosion resistance (electrochemical corrosion, intergranular corrosion, etc.) of the as-extruded AA7055 helical profile.

2 Experimental

2.1 Extrusion tests and sample preparation

The AA7055 extrusion billet used in this work is d118 mm × 350 mm and its chemical composition is listed in Table 1. In order to effectively reduce the casting stress and segregation, the alloy was homogenized at 468 °C for 24 h.

Table 1 Chemical composition of AA7055 (wt.%)

Zn	Mg	Cu	Zr	Ti
8.03	2.08	2.22	0.12	0.03
Fe	Si	Mn	Cr	Al
<0.01	<0.01	<0.01	<0.01	Bal.

The extruded profile studied in this work is a three-bladed helical profile and the extrusion die was designed and manufactured in our previous work [29]. After homogenization, the billet was extruded in a 1000 t press with an extrusion ratio of 5.8, using the billet and die temperature of 420 °C, and extrusion speed of 0.3 mm/s. After experiment, the extruded profile was immediately quenched into cold water. The extrusion die and the extruded profile are shown in Fig. 1.

In order to investigate and compare consistently the effects of the solid solution treatments on the microstructure and mechanical properties of the profile, all testing samples were taken from the core of the profile, as shown in Figs. 2 and 3.

2.2 Determination of solid solution schemes
2.2.1 DSC analysis

In order to determine the temperature range of solid solution treatment, differential scanning calorimetry (DSC) analyses were carried out at a heating rate of 10 °C/min for the extruded sample, as shown in Fig. 4. It was seen that there were two endothermic peaks at 474.4 and 484.1 °C, respectively. In addition, according to the Refs. [30−33], the melting points of the η, T and S phases are approximately 470−475, 482 and 490−501 °C. For above analysis, the experimental scheme of solid solution treatments was determined in this work as listed in Table 2.
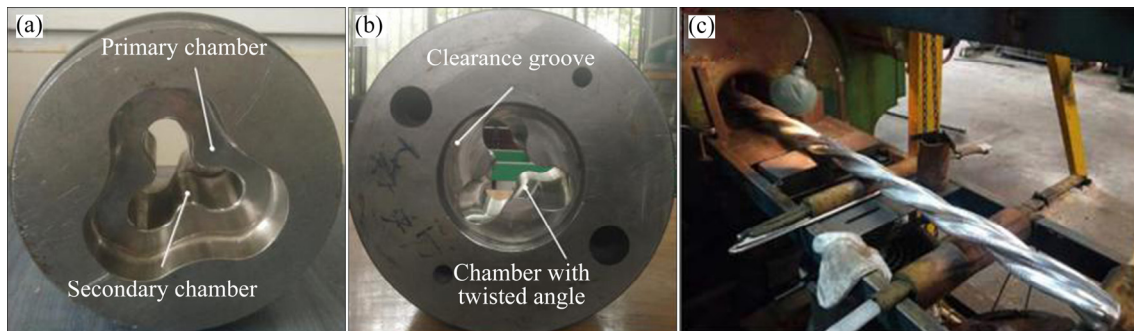

Fig. 1 Extrusion die and extruded helical aluminum profile: (a) Prechamber; (b) Twisted die; (c) Extruded profile
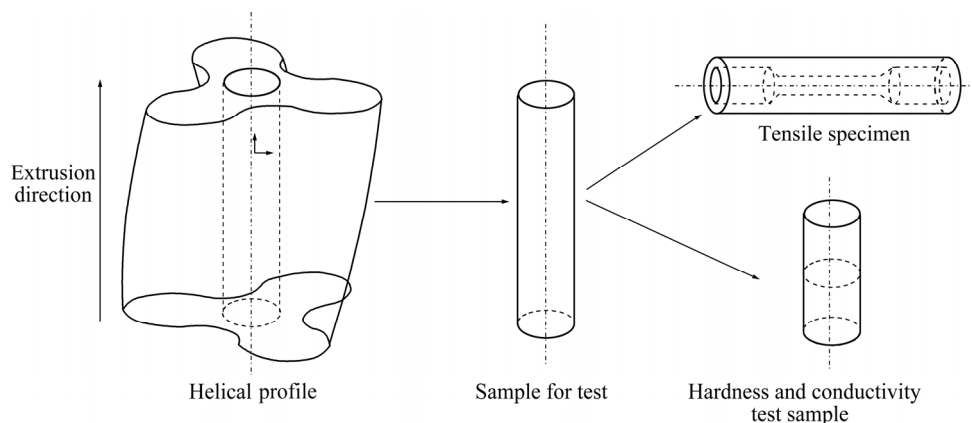

Fig. 2 Specimen preparation for tensile, hardness and conductivity experiments
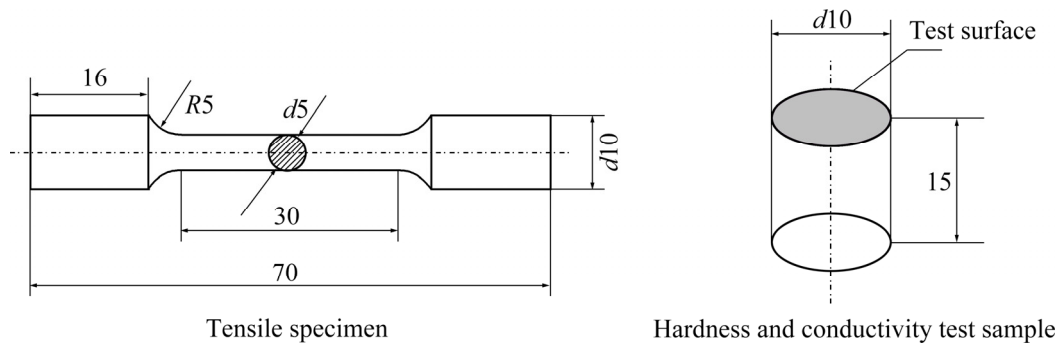
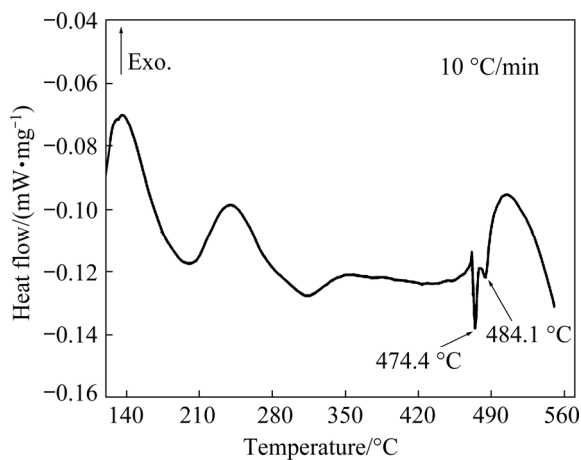Fig. 3 Dimensions of tensile, hardness and conductivity specimens (unit: mm)

Fig. 4 DSC curve of AA7055 extruded profile

Table 2 Four solid solution treatment schemes studied in this work

Solution scheme	First stage	Second stage	Third stage	Fourth stage
SST	470 °C, 60 min			
EST	460 °C, 45 min	480 °C, 15 min		
HTPP	460 °C, 45 min	480 °C, 15 min	420 °C, 15 min	
MST	200 °C, 60 min	300 °C, 60 min	400 °C, 60 min	470 °C, 15 min

2.2.2 Determination of experimental scheme

According to our previous study, the peak tensile strength reached a maximum of 683 and 695 MPa after SST of (470 °C, 60 min) and EST of (460 °C, 45 min + 480 °C, 15 min), respectively. Here to systematically compare the influence of HTPP and MST on the microstructure and mechanical properties of AA7055, the above SST and EST schemes were chosen as a basis. For HTPP, a slightly reduced-temperature solution (420 °C, 15 min) was carried out after EST, while the MST scheme with four heating and holding stages was chosen, as shown in Table 2. After each solid solution treatment, the water-quenched samples were aged at 120 °C for 24 h.

2.3 Material characterization

The composition, quantity, distribution and tensile fracture morphology of the second-phase precipitates after the solid solution treatment were observed by scanning electron microscopy and energy dispersive spectroscopy (SEM-EDS) analysis with JSM−7800F.

Grain orientation and texture evolution analysis were performed using Oxford Nordlys Max3 backscattered electron diffraction (EBSD) system. The samples were electro-polished in electrolyte (10 mL perchloric acid + 90 mL alcohol). The electrolytic voltage was 30 V, the current was 0.7 A, and the electrolytic time was 5 s.

The type and morphology of the second-phase precipitates at the GBs were observed by JEM−2100 high-resolution transmission electron microscopy (HRTEM). The TEM sample was observed by electron microscopy after being double-sprayed for thinning by methanol (volume ratio of 3:7).

Electrochemical corrosion (EC) performance was tested with a 3.5 wt.% NaCl solution. The scanning frequency range was $10^{-2}-10^5$, and the disturbance amplitude was 0.01 V. In the polarization curve test, the scanning range was open circuit potential ±0.2 V, the scanning speed was 0.001 V/s and the sensitivity was 10^{-3}.

The intergranular corrosion (IGC) performance testing was carried out with the sample size of $d13$ mm × 40 mm. The sample was pretreated with

10% NaOH solution and 30% HNO$_3$ solution, then placed in the corrosive solution for 6 h. The temperature of the corrosive solution was controlled at (35±2) °C.

3 Results and discussion

3.1 Microstructural analysis

3.1.1 Second-phase particles distribution

Figure 5 shows the distribution of the second-phase particles of the as-quenched alloy under four different solid solution regimes. The compositions of the second-phase particles were analyzed by EDS to determine their phase types, as displayed in Fig. 6. Combined with Figs. 5 and 6, it can be found that there are three kinds of main residual phases in the alloy after solid solution treatment: T phase (AlZnMgCu), S phase (Al$_2$CuMg) and Fe-containing impurity phase Al$_7$Cu$_2$Fe. From Fig. 5(a), it was observed that there were still many coarse S phase particles and a few rod-shaped T phase particles in the alloy after SST, indicating that the large-size S phase particles were difficult to dissolve at low temperatures, while the T phase particles were relatively easy to dissolve. But the S phase particles would largely dissolve after EST (Fig. 5(b)) and a small amount of fine Fe-containing impurity phase Al$_7$Cu$_2$Fe was found. Compared

with SST, the morphology of the phases became more irregular but more compact, the size was smaller, the distribution was more dispersed, and more coarse second-phase particles were dissolved after EST. From the distribution of the second-phase particles under the HTPP in Fig. 5(c), it was seen that quantities of second-phase particles (especially T phase) precipitated in the third stage, and were intermittently distributed at the GBs. After MST, the remaining second-phase particles were fine and diffuse, as shown in Fig. 5(d). There were still a certain number of small T phase and S phase particles, which was possibly caused by the lower solution temperature (470 °C) and shorter holding time (15 min) in the last stage, but the solution effect had been significantly improved in general.

Figure 7 shows the statistics of the second-phase particles under different solution regimes based on the ImageJ software. Compared with SST, the second phases were further dissolved after EST, and the number of second-phase particles, the area fraction, and the average diameter were significantly reduced. After HTPP, the number and area fraction of the second-phase particles increased significantly, but their size was smaller. As shown in Fig. 5(a), the undissolved phase after SST was dominated by the coarse S phase, which might be the reason why the average diameter of the second-
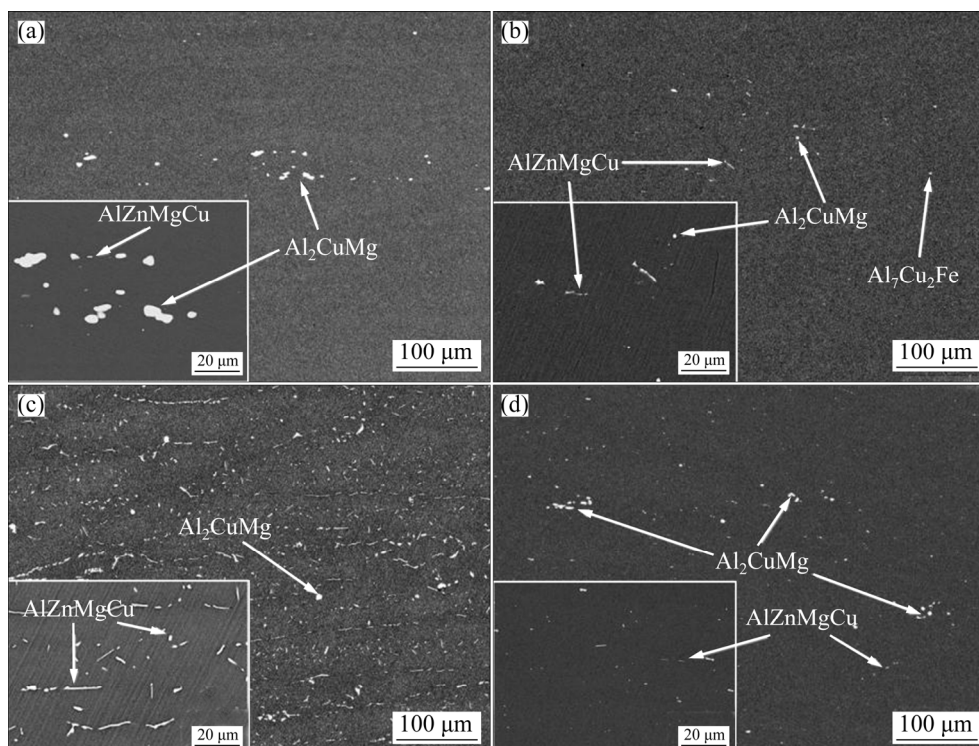

Fig. 5 Second-phase distribution after different solid solution treatments: (a) SST; (b) EST; (c) HTPP; (d) MST
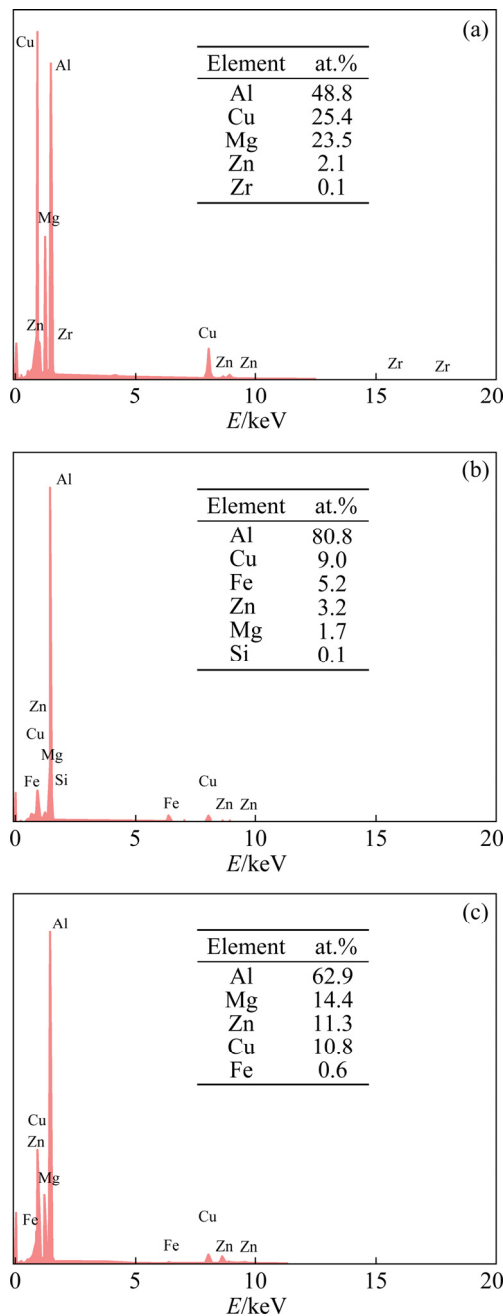
Fig. 6 EDS spectra of second-phase particles: (a) S phase (Al₂CuMg); (b) Al₇Cu₂Fe phase; (c) T phase (AlZnMgCu)

Fig. 7 Statistical results of second phases after different solid solution treatments: (a) Number of particles; (b) Area fraction; (c) Average diameter

phase particles after HTPP was smaller than that after SST, as plotted in Fig. 7(c). For MST, the number, the area fraction and the average diameter of second-phase particles were all between SST and EST. The above analysis showed that EST and MST improved the solid solution effect obviously compared to SST, and HTPP brought a large number of precipitated phases in the third stage.

It was indicated that the width of the grain boundary precipitation-free zone (PFZ), the size
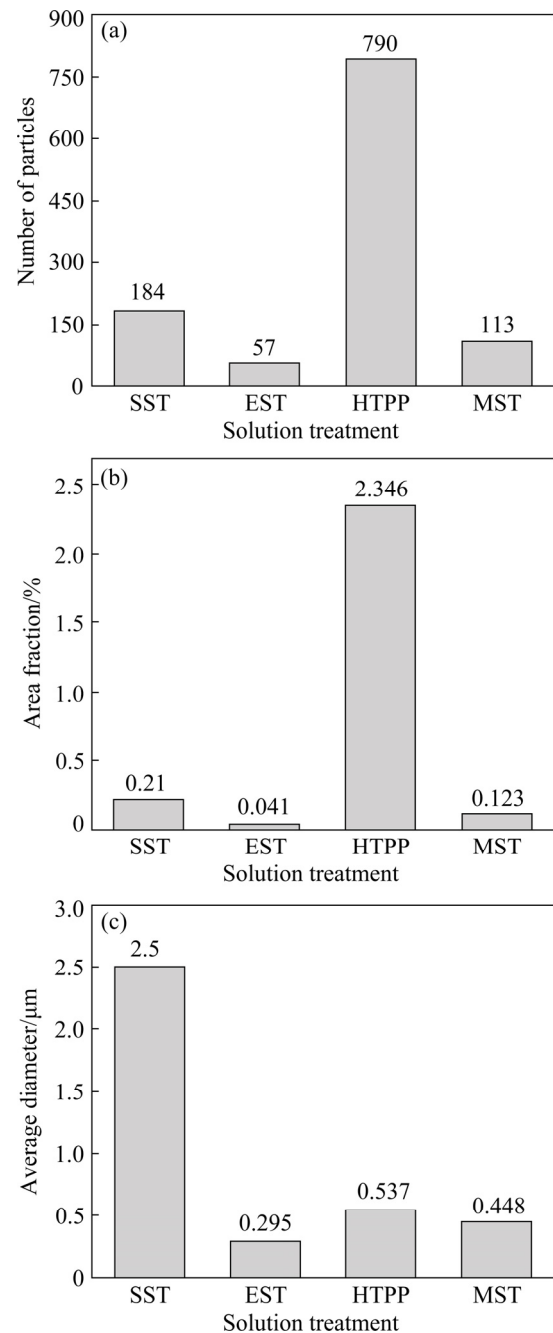
and spacing of the second phases at the GBs could affect the corrosion resistance of the aluminum alloy [16]. Figure 8 compares the morphology of the second-phase particles at the GBs after different solid solution treatments. It was observed that the precipitates were uniformly distributed inside the grains, but the solid solution treatment had a significant effect on the morphology of the second phases at the GBs. After SST, the second-phase particles at the GBs were larger and more
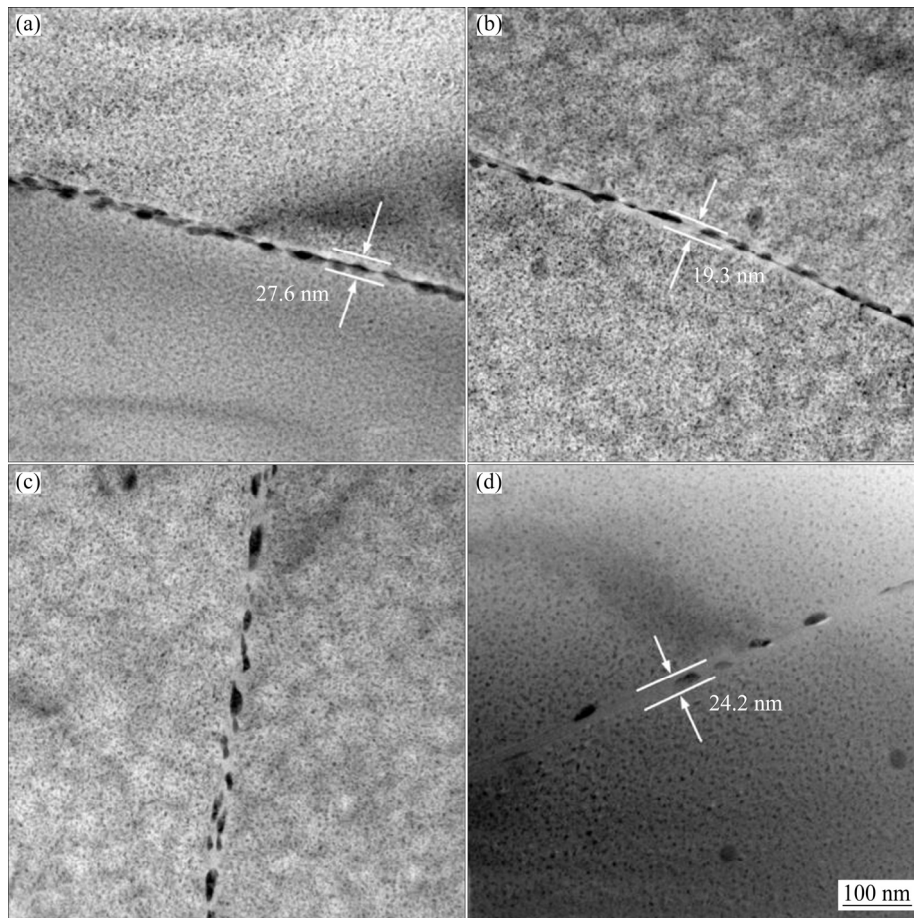
Fig. 8 Distribution of second phases at GBs after different solid solution treatments: (a) SST; (b) EST; (c) HTPP; (d) MST

continuously distributed along the GBs, and the width of the PFZ was about 27.6 nm. By comparison, the distribution of the second-phase particles did not significantly change after EST. The distribution of the intergranular phases was not uniform, and even presented the continuous distribution in some regions. In addition, the width of the PFZ decreased to about 19.3 nm after EST. For HTPP, the size of the second-phase particles intermittently distributed at the GBs increased significantly, but no obvious PFZ was found. However, the size of the second-phase particles at the GBs became smaller after MST, the space between the phases was significantly increased, and the width of the PFZ was approximately 24.2 nm.

3.1.2 Grain orientation and morphology

Figure 9 shows the grain orientation distribution and morphology of the as-extruded alloy and the alloy after different solid solution treatments. The black and white lines in the figure respectively represent high-angle grain boundaries (HGBs, the orientation angle between neighbouring

grains is greater than 15°) and low-angle grain boundaries (LGBs, the orientation angle is between 2° and 15°). The as-extruded grains were strip-like and distributed along extrusion direction (ED), and there were a lot of fine sub-grains inside, which indicated that a large number of dislocations were generated by the severe deformation during the extrusion process. And the recrystallization occurred at this time, since many fine grains were found at the junction of different long strip-like grains. For all treatments, the grains were generally long strips and mainly distributed along the directions of ⟨001⟩ and ⟨111⟩ parallel to ED. After SST, the grains were still slender and strip-like, and there were many high-angle recrystallized grains at the GBs, while the grains grew obviously after EST and HTPP. Higher solution temperature or longer holding time might cause the aspect ratio to be significantly smaller, as observed in the work of TRIPATHI et al [34]. After MST, the grain growth was obviously reduced compared to EST and HTPP, as shown in Fig. 9(i).
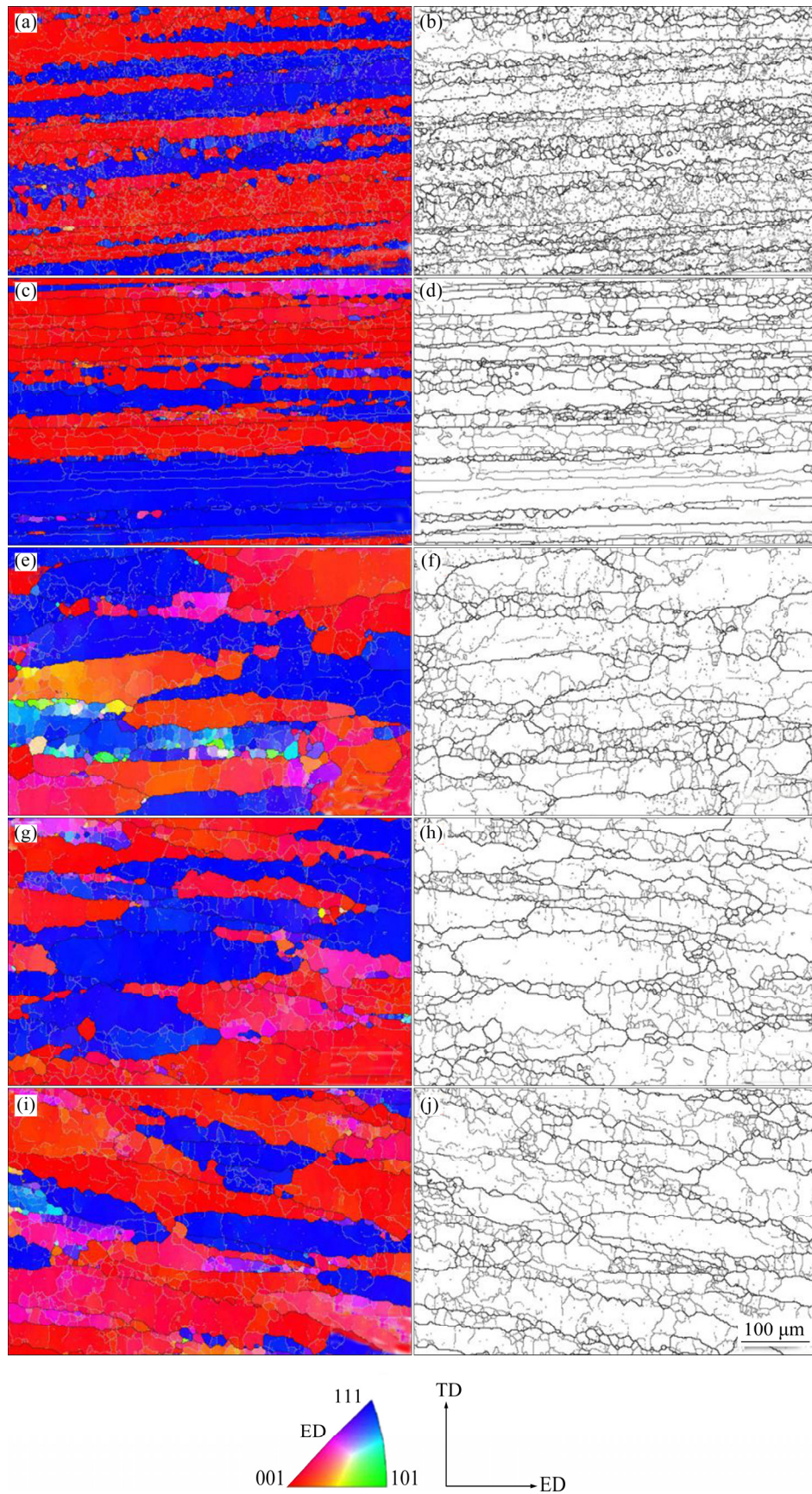
Fig. 9 Orientation distribution and grain morphology before and after different solid solution treatments: (a, b) As-extruded; (c, d) SST; (e, f) EST; (g, h) HTPP; (i, j) MST

Figure 10 shows the distribution of grain orientation difference under different solid solution regimes. The proportion of LGBs was much higher for EST (54.69%), HTPP(48.68%) and MST(57.24%) than for SST(29.59%). The increase in grain size and LGBs could be attributed to the increase in solution temperature or holding time. Combined with Fig. 9, it can be found that the number of fine equiaxed grains after SST was significantly higher than that in the other three solution schemes, which indicated that the abundant recrystallization occurred at a LGBs ratio of 29.59%. As discussed by HUANG et al [35], fine dispersions retarded the recrystallization by pinning (sub)boundary migration while coarse particles could accelerate the recrystallization through the particle stimulated nucleation. There remained quantities of coarse compositions with relatively large spacing in the alloy (Fig. 5(a)), around which the strong deformation zone could provide nucleation point and driving force for the recrystallization. However, the other three systems mainly prevented dislocation climbing and slippage due to the Zener pinning effect of fine dispersed phase particles, which limited the migration of the GBs, providing insufficient conditions for recrystallization. For MST, the recrystallization could be effectively inhibited by consuming deformation energy during the low-temperature holding stages, so its grain size was smaller, and plenty of low-angle sub-grains were observed in the long-strip grains.

3.1.3 Crystallographic texture

The inverse pole figures (IPF) of the alloy under four solid solution treatments are shown in Fig. 11. Combined with Fig. 9, it was seen that the extruded grains of alloy were elongated after SST, mainly distributed along the ⟨001⟩ and ⟨111⟩ directions parallel to ED, and the orientation distribution density was 20.44. While the grain orientation was weakened to a certain extent after EST, HTPP and MST, accompanied by a significant decrease in the density of the maximum orientation distribution. In addition, the grain orientations under different solid solution treatments were different. The grains treated by EST and HTPP tended to be distributed along ED ⟨111⟩, while the grains after MST tended to be along ED ⟨001⟩.

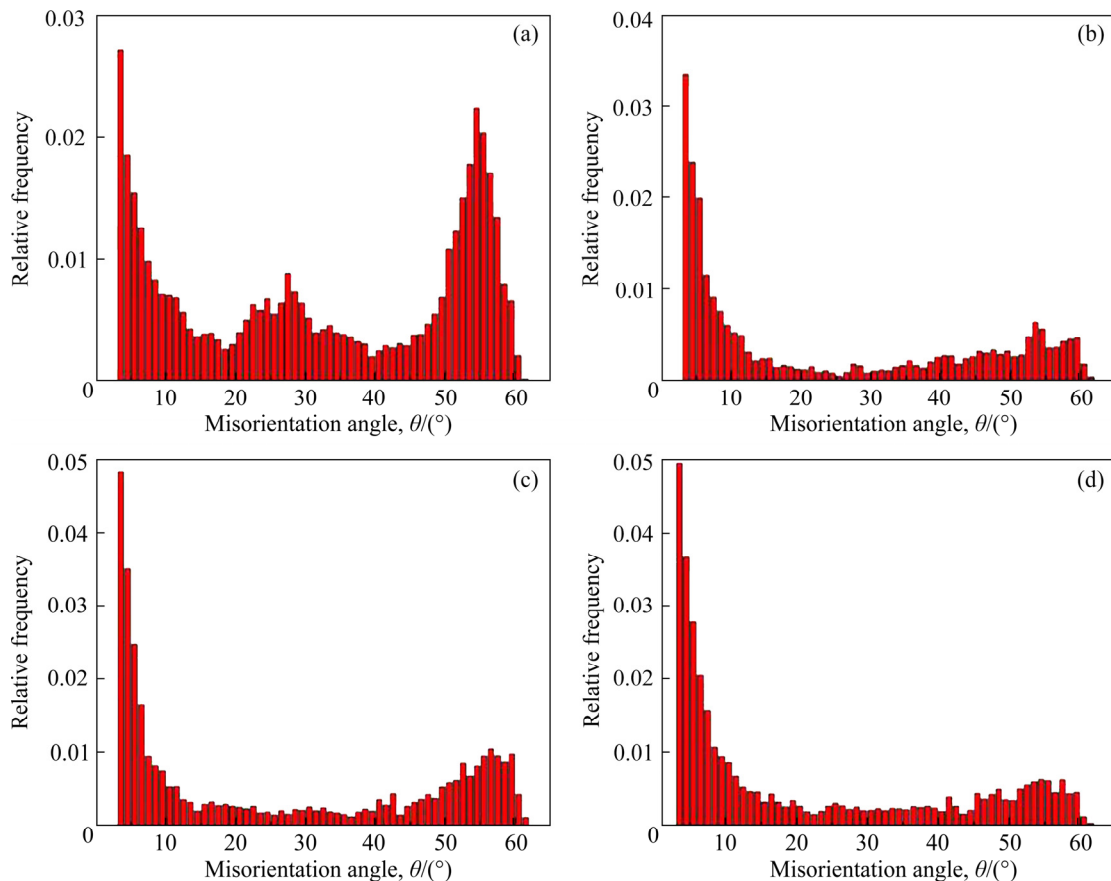**Fig. 10** Misorientation distribution of grain boundary after different solid solution treatments: (a) SST; (b) EST; (c) HTPP; (d) MST

⟨112⟩), Goss ({110}⟨001⟩), Cube ({100}⟨100⟩), and Copper ({112}⟨111⟩) textures. After SST, the alloy was mainly composed of Copper, Goss and Cube textures, and its texture strength was significantly higher than those after other solid solution treatments. Compared to SST, the texture strength after EST was weakened, and a small amount of Brass texture appeared. The texture type after HTPP was basically the same as that after EST, but the texture strength was obviously improved. After MST, there was no Goss texture, and both Copper texture and Brass texture were weakened. Since most of the grains were distributed along ED ⟨001⟩, as shown in Fig. 9(i) and Fig. 11(d), only the strong Cube texture existed in the alloy after MST (Fig. 12(d)).

3.2 Conductivity and mechanical properties

Figure 14 shows the hardness and conductivity of the as-quenched and as-aged AA7055 under different solid solution treatment regimes. The corresponding tensile properties of the as-aged alloy are shown in Fig. 15. For as-quenched alloy, the hardness gradually decreased from SST to EST to MST. This might result from that the dissolution of reinforcing phases reduced the pinning effect of the second-phase particles on the dislocations, and
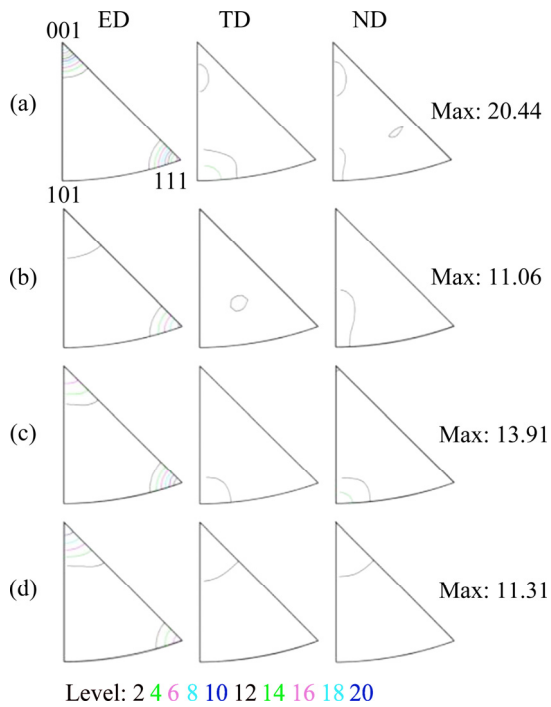

Fig. 11 IPF maps after different solid solution treatments: (a) SST; (b) EST; (c) HTPP; (d) MST

The orientation distribution function (ODF) maps are shown in Fig. 12. Compared with the standard ODF diagram at $\varphi_2=45°$ in Fig. 13, it was seen that the alloy mainly contained Brass ({110}
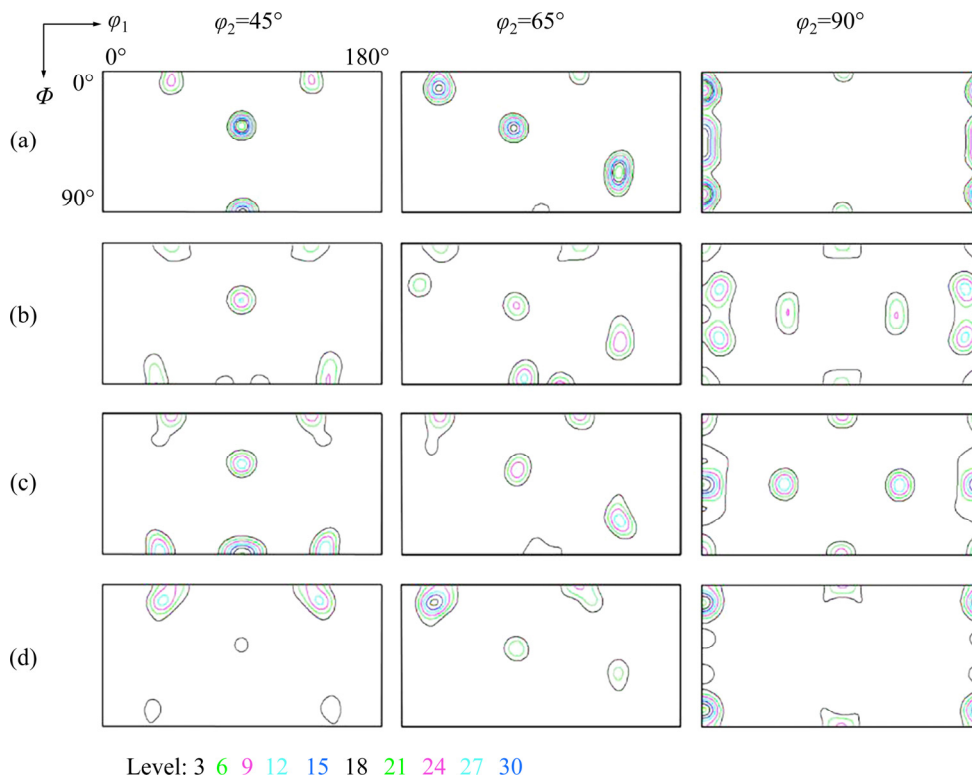

Fig. 12 ODF maps after different solid solution treatments: (a) SST; (b) EST; (c) HTPP; (d) MST
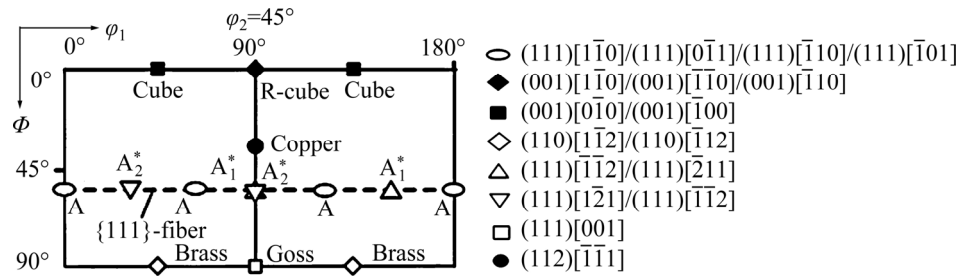
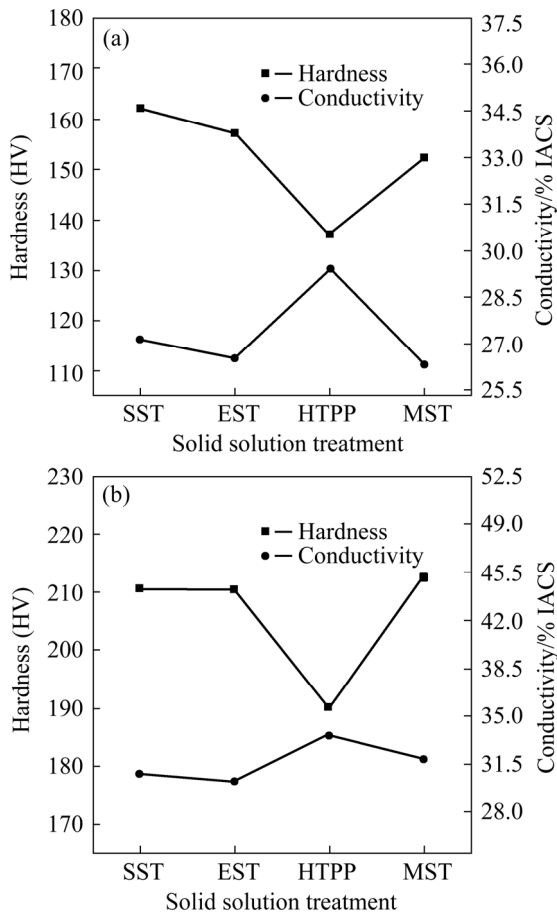**Fig. 13** Standard ODF map (φ_2=45°)

Fig. 14 Effect of solid solution treatment on hardness and conductivity of AA7055: (a) As-quenched alloy; (b) As-aged alloy

impaired the mechanical properties of material. While the hardness after HTPP was the lowest, since a large number of precipitated phases reduced the concentration of the alloy elements in the matrix, and the strength of the alloy was also reduced. The conductivity of the alloy was mainly controlled by the phases of high conductivity. The increase of the solid solubility of the matrix, i.e., the increase of the concentration of alloy elements in the matrix, resulted in the decrease in the conductivity. As shown in Fig. 14(a), the conductivity gradually
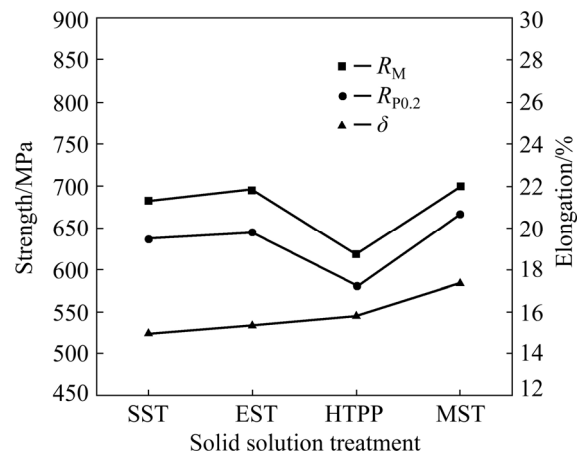

Fig. 15 Strength and elongation of as-aged AA7055 under different solid solution treatments

decreased from SST to EST to MST. Owing to the precipitation action of HTPP and impoverishment of solute atoms in the matrix, the conductivity was obviously increased accordingly.

In the as-aged alloy, there was no obvious difference in conductivity, though HTPP still got the highest conductivity, followed by MST, which might result from the increase of the number of precipitated phases and the decrease of matrix supersaturation during the aging treatment process. At the same time, the distribution difference of precipitated phases also decreased. As shown in Fig. 14(b) and Fig. 15, the as-aged alloy after HTPP had the lowest hardness and strength. This implied that the weakening effect of HTPP on the mechanical properties of the alloy was evident, which was because quantities of second-phase particles were precipitated in the matrix, leading to the greater loss of vacancies and solute atoms in matrix. And the effect of subsequent aging strengthening was weakened severely, as a result. At the same time, due to the prolongation of solid solution time, the recrystallized grains would grow up, which was also harmful to the strength of the

alloy. Whereas the alloy after MST had the highest hardness and strength, followed by EST. Because the solution effect of these two schemes was greatly improved, the coarse undissolved crystalline phases were greatly reduced (Fig. 5), and the supersaturation degree of the alloy after quenching was greatly improved, compared with SST. During the following aging stage, the optimization of the number and distribution of precipitated phases was beneficial to the increase of mechanical properties. In addition, as shown in Fig. 12, both the strong Copper texture under EST system and the strong Cube texture under MST system might bring favorable effects on the strength of the alloy along ED.

The fracture usually occurs near coarse constituents as the sources of micro-crack and then links up along the matrix and GBs [16]. As a result, it can be seen from the elongation curve in Fig. 15, the elongation after SST was the lowest, about 15.0%, while the elongation was up to 15.4% after EST due to the small volume fraction and size of the constituents. After HTPP, the elongation was improved to some extent, approximately 15.8%, though the aging strengthening effect of the alloy was weakened. This might be related to the uniform distribution of fine precipitated phase particles, against the generation and expansion of the cracks. After MST, the alloy obtained the best elongation of 17.4%.

Figure 16 shows the fracture morphology of tensile samples after different solid solution treatments. It can be seen from the figure that there were dimples of different sizes and intergranular cracks on the tensile fracture. Besides, the coarse dimples contained secondary component particles, which was identified previously [20]. After SST, the cleavage characteristics were very obvious, and the number of dimples was quite small, which might mean a lower elongation under this condition. After EST, the fracture was composed of the large cleavage planes and the small dimples between the cleavage planes, which indicated that the elongation of the alloy could be improved to a certain extent. In addition, the dimples of the alloy after HTPP were smaller and more uniform than those of SST, which might reflect the increase of elongation. After MST, the short-bending tearing edges, trans-granular cracks and a small number of cleavage steps were observed, and fine dimples

were distributed between the tearing ribs. In general, MST and HTPP resulted in relatively uniform deformation of the grains during the tensile process, generating a large number of small dimples, and the early fracture stemming from the coarse phases was avoided, so that the elongation was improved, as plotted in Fig. 15.

3.3 Corrosion resistance

3.3.1 Electrochemical corrosion

Figure 17(a) shows the relationship between open-circuit potential (OCP) and soaking time in 3.5 wt.% NaCl solution of AA7055 after different solid solution treatments and the corresponding polarization curves are shown in Fig. 17(b). The corrosion parameters (self-corrosion potential φ_{corr} and self-corrosion current density J_{corr}) obtained by Tafel extrapolation are listed in Table 3. The magnitude of OCP reflects the corrosion resistance of the alloy in a certain medium environment. The more negative the OCP is, the more susceptible the alloy is to corrosion [36]. It was seen that the magnitude of OCP of each sample increased gradually, and finally stabilized at a certain value. The OCP after MST was the highest, −0.76 to −0.75 V, followed by HTPP and SST, which fluctuated around −0.76 V. After EST, the magnitude of OCP was the lowest, between −0.81 and −0.79 V. As a whole, the alloy after MST seemed to have the best corrosion resistance. In addition, the lower the self-corrosion potential is, the greater the corrosion tendency gets, and the greater the self-corrosion current density is, the faster the corrosion rate gets. Combined with Fig. 17(b) and Table 3, the alloy after HTPP and MST had a higher corrosion resistance than that after SST and EST.

As shown in Fig. 17(a), the value of the OCP in the curve is initially low, due to the fact that the region of initial attack from the corrosive medium might be where the second phases segregate severely, such as the region where the coarse phases aggregate or wrap each other. The enrichment of Cu and the positive shift of OCP were caused by the dealloying of the second phases after corrosion, leading the decrease of oxidation reaction force. On the other hand, the corrosion products hindered the further corrosion through the corrosion medium. Therefore, the OCP curve rose first and reached stability gradually as shown in Fig. 17(a). The
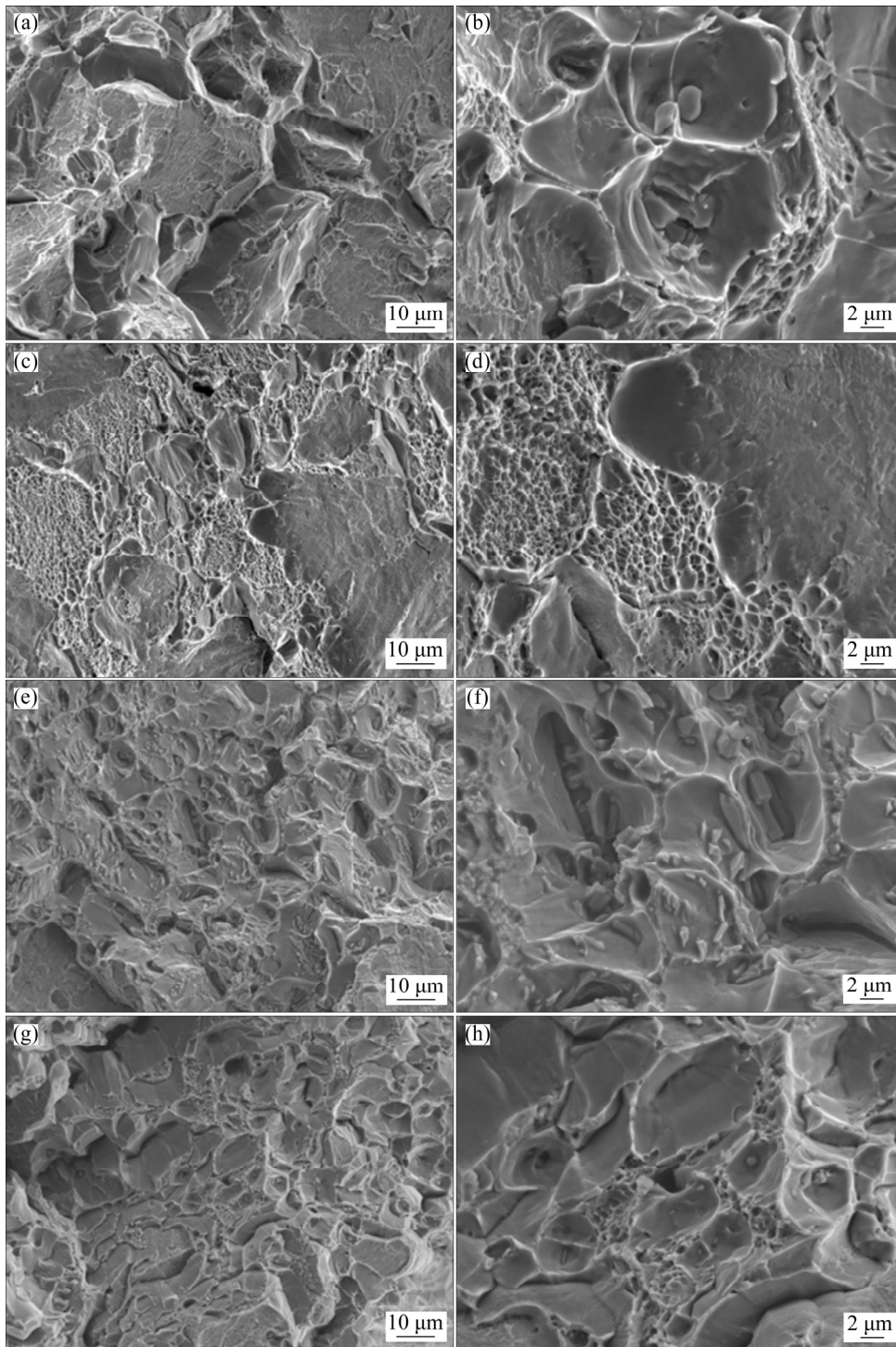
Fig. 16 Tensile fracture morphology after different solid solution treatments: (a, b) SST; (c, d) EST; (e, f) HTPP; (g, h) MST

solution effect of the alloy after SST was relatively poor, manifesting that a large number of coarse and uneven second-phase particles remaining. As a result, the number of the micro-batteries was large, causing the poor EC performance. Although the solution effect of EST was improved, the blocking effect of the grain boundary's corrosion products

was reduced due to the non-uniformity of the intergranular phases after EST (Fig. 8(b)). Consequently, the grain boundary became an anode corrosion channel, and the corrosion resistance was decreased. In addition, HTPP and MST achieved a good matching between the matrix and second phases by regulating the dissolution and
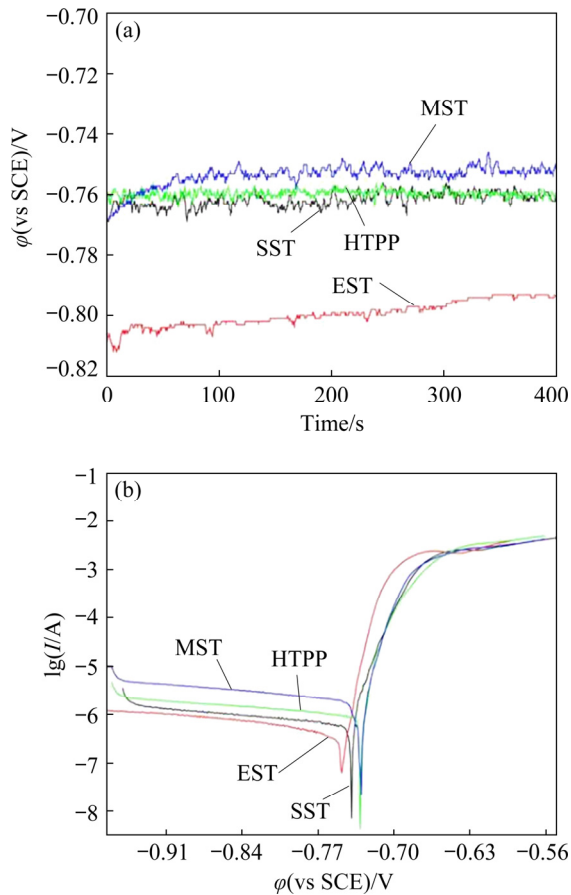
Fig. 17 Electrochemical corrosion analysis of alloy: (a) OCP curves of alloy after different solid solution treatments; (b) Polarization curves after different solid solution treatments

Table 3 Corrosion parameters after different solid solution treatments

Treatment	φ_{corr}(SCE)/V	J_{corr}/(10^{-7} A·cm^{-2})
SST	−0.7371	6.41
EST	−0.7488	7.21
HTPP	−0.7313	1.50
MST	−0.7308	2.94

precipitation of the second phases. The non-uniformity of the electrochemical properties between the GBs and the grains was reduced, resulting in the improvement of corrosion resistance.

3.3.2 Intergranular corrosion (IGC)

According to Ref. [24], the corrosion potential (φ_{corr}) of the PFZ and Al matrix was positive compared with the η phase at the GBs. Therefore, the η phase was always anode relative to the Al

matrix and the PFZ, resulting in η phase dissolution and IGC. Figure 18 shows the IGC morphology and the maximum corrosion depth after different solid solution treatments. It was found that the solid solution treatment had great influence on IGC. The IGC depth after EST was the largest, about 154 μm, while the minimum depth of 100 μm was observed in the alloy after MST. The resistance of the alloy to IGC after different solid solution treatments was ordered as: MST>HTPP>SST>EST. Due to the lower temperature (420 °C) process of the third stage in the HTPP system, the equilibrium phases had a strong tendency to precipitate at the GBs. As shown in Fig. 8(c), the HTPP could increase the size, spacing and distribution of the GBPs, and the GBPs got coarsened and dispersed, which was beneficial for the IGC performance. For MST, the improved corrosion resistance of the alloy could result from the increased spacing of the GBPs and inhibited recrystallization. However, the IGC performance of the alloy after EST was relatively poor, which might not achieve a good regulation of the intergranular phases. As shown in Fig. 8(b), and the intergranular phases were in a relatively continuous distribution state, which was even more obvious than that after SST in partial regions.

4 Conclusions

(1) Quantities of undissolved S and T phases were observed after SST, while the undissolved phases after EST were significantly reduced. For HTPP, a large number of second-phase particles (mainly T phase) were precipitated in the solution stage, and the coarse second-phase particles at the GBs were distributed discontinuously. For MST, small-size T and S phase particles remained and the second phases at the GBs were more dispersed than those for HTTP.

(2) There were many high-angle recrystallized grains at the GBs after SST. The texture was mainly high-strength Copper, Goss and Cube. After EST, the grain size increased, the proportion of LGBs increased, the strength of each texture decreased obviously, and at the same time, a small amount of Brass texture appeared. Compared with EST, the proportion of LGBs decreased after HTPP, while the texture strength increased. However, after MST, the proportion of the LGBs was the highest, and the texture strength was also maintained at a high level.
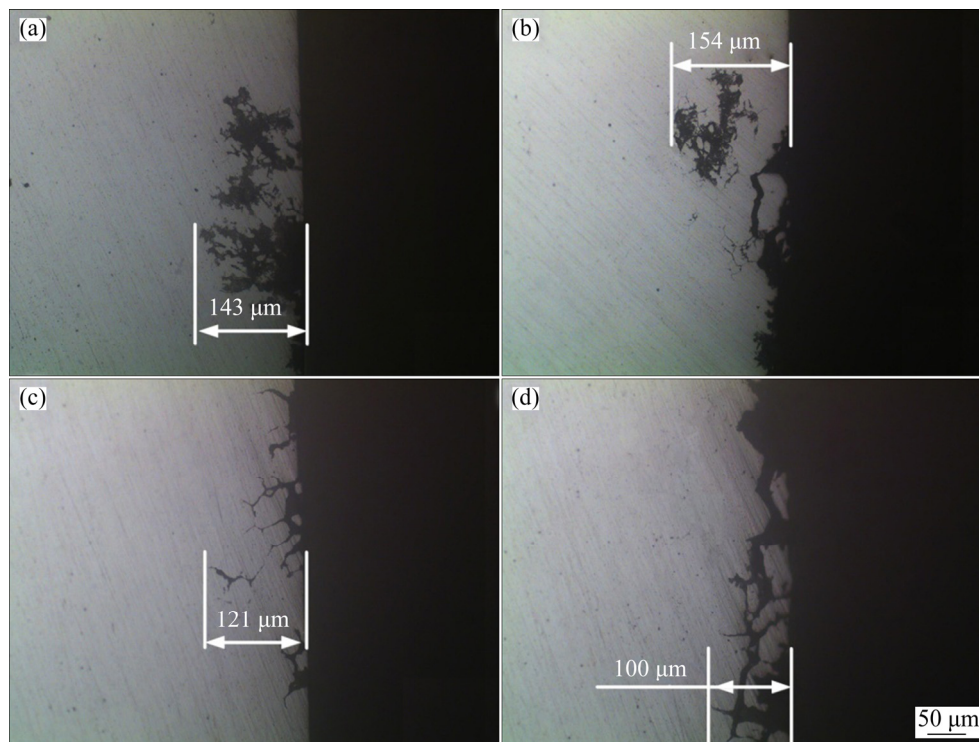
Fig. 18 Morphologies of intergranular corrosion after different solid solution treatments: (a) SST; (b) EST; (c) HTPP; (d) MST

(3) Compared to SST, the as-quenched alloy under EST had lower hardness and conductivity, while the strength and elongation both increased. Though the elongation of the alloy after HTPP increased, its tensile strength and yield strength decreased significantly compared to that after SST and EST. The best mechanical properties of the alloy were obtained after MST: the hardness was HV 212.5, the tensile strength was 700 MPa, the yield strength was 667 MPa, and the elongation was 17.4%.

(4) HTPP and MST significantly improved the corrosion resistance of the alloy. The conductivity of the alloy after MST was 31.9% IACS, the open circuit potential was about −0.76 V, the self-corrosion potential was −0.7308 V, the self-corrosion current density was 2.94×10^{-7} A/cm^2, and the maximum intergranular corrosion depth was approximately 100 μm. Therefore, considering the mechanical properties and corrosion resistance, MST was the best solid solution treatment for AA7055.

Acknowledgments

References

[1] WILLIAMS J C, STARKE E A. Progress in structural materials for aerospace systems [J]. Acta Materialia, 2003, 51(19): 5775−5799.

[2] ROMETSCH P A, ZHANG Y, KNIGHT S. Heat treatment of 7xxx series aluminium alloys-Some recent developments [J]. Transactions of Nonferrous Metals Society of China, 2014, 24(7): 2003−2017.

[3] de SALVO J G J, AFONSO C R M. Fatigue strength and microstructure evaluation of Al 7050 alloy wires recycled by spray forming, extrusion and rotary swaging [J]. Transactions of Nonferrous Metals Society of China, 2020, 30(12): 3195−3209.

[4] KHALIFA N B, TEKKAYA A E. Newest developments on the manufacture of helical profiles by hot extrusion [J]. Journal of Manufacturing Science and Engineering, 2011, 133(6): 061010.

[5] CHEN Gao-jin, CHEN Liang, ZHAO Guo-qun, ZHANG Cun-sheng. Microstructure evolution during solution treatment of extruded Al−Zn−Mg profile containing a longitudinal weld seam [J]. Journal of Alloys and Compounds, 2017, 729: 210−221.

[6]   LI Bo, PAN Qing-lin, CHEN Cong-ping, WU Hai-hua, YIN Zhi-min. Effects of solution treatment on microstructural and mechanical properties of Al−Zn−Mg alloy by microalloying with Sc and Zr [J]. Journal of Alloys and Compounds, 2016, 664: 553−564.

[7]   YANG Wen-chao, JI Shou-xun, WANG Ming-pu, LI Zhou. Precipitation behaviour of Al−Zn−Mg−Cu alloy and diffraction analysis from η' precipitates in four variants [J]. Journal of Alloys and Compounds, 2014, 610: 623−629.

[8]   USTINOVSHIKOV Y I. Precipitation in solids [J]. Journal of Materials Science, 1992, 27(15): 3993−4002.

[9]   SRIVATSAN T S, ANAND S, SRIRAM S, VASUDEVAN V K. The high-cycle fatigue and fracture behavior of aluminum alloy 7055 [J]. Materials Science and Engineering A, 2000, 281(1−2): 292−304.

[10] COSTA T A, DIAS M, GOMES L G, ROCHA O L, GARCIA A. Effect of solution time in T6 heat treatment on microstructure and hardness of a directionally solidified Al−Si−Cu alloy [J]. Journal of Alloys and Compounds, 2016, 683: 485−494.

[11] HU Xie-jun, ZHANG Ren-guo, ZHANG Xiao-yan, LIN Ting-yi, ZHANG Jun-jie, YAN Jun. Effects of progressive solution treatment on microstructure and property of the aluminium alloy electrical round rod [J]. IOP Conference Series: Materials Science and Engineering, 2017, 207: 012060.

[12] WANG Xiao-feng, GUO Ming-xing, CHAPUIS A, LUO Jin-ru, ZHANG Ji-shan, ZHUANG Lin-zhong. Effect of solution time on microstructure, texture and mechanical properties of Al−Mg−Si−Cu alloys [J]. Materials Science and Engineering A, 2015, 644: 137−151.

[13] HAN N M, ZHANG X M, LIU S D, HE D G, ZHANG R. Effect of solution treatment on the strength and fracture toughness of aluminum alloy 7050 [J]. Journal of Alloys and Compounds, 2011, 509(10): 4138−4145.

[14] PENG Guo-sheng, CHEN Kang-hua, CHEN Song-yi, FANG Hua-chan. Evolution of the second phase particles during the heating-up process of solution treatment of Al−Zn−Mg−Cu alloy [J]. Materials Science and Engineering A, 2015, 641: 237−241.

[15] DIMAS P P, BONDAN T S. Effect of solution treatment temperature on the microstructure and mechanical properties of Al−5.1Zn−1.9Mg alloy produced by squeeze casting [J]. IOP Conference Series: Materials Science and Engineering, 2018, 432: 12064.

[16] SONG Min, CHEN Kang-hua. Effects of the enhanced heat treatment on the mechanical properties and stress corrosion behavior of an Al−Zn−Mg alloy [J]. Journal of Materials Science, 2008, 43(15): 5265−5273.

[17] GERARD M L, DAVID E L. The influence of microstructure and strength on the fracture mode and toughness of 7xxx series aluminum alloys [J]. Metallurgical Transactions A, 1982, 13(3): 411−425.

[18] LIAO Bin, CAO Ling-fei, WU Xiao-dong, ZOU Yan, HUANG Guang-jie, ROMETSCH P, COUPER M J, LIU Qing. Effect of heat treatment condition on the flow behavior and recrystallization mechanisms of aluminum alloy 7055 [J]. Materials, 2019, 12(2): 311.

[19] SOKOLOWSKI J H, SUN X C, BYCZYNSKI G, NORTHWOOD D O, PENROD D E, THOMAS R, ESSELTIBE A. The removal of copper-phase segregation and the subsequent improvement in mechanical properties of cast 319 aluminium alloys by a two-stage solution heat treatment [J]. Journal of Materials Processing Technology, 1995, 53(1−2): 385−392.

[20] CHEN Kang-hua, LIU Hong-wei, ZHANG Zhuo, LI Song, RICHARD I T. The improvement of constituent dissolution and mechanical properties of 7055 aluminum alloy by stepped heat treatments [J]. Journal of Materials Processing Technology, 2003, 142(1): 190−196.

[21] KONGIANG S, PLOOKPHOL T, WANNASIN J, WISUTMETHANGOON S. Effect of the two-step solution heat treatment on the microstructure of semisolid cast 7075 aluminum alloy [J]. Advanced Materials Research, 2012, 488−489: 243−247.

[22] PENG Xiao-yan, LI Yao, GUO Qi, XU Guo-fu. Effects of enhanced solution treatment on stress corrosion behavior of Al−Zn−Mg−Cu alloy [J]. Journal of the Minerals, Metals & Materials Society, 2018, 70(11): 2692−2697.

[23] CHEN Kang-hua, HUANG Lan-ping. Effect of high-temperature pre-precipitation on microstructure and properties of 7055 aluminum alloy [J]. Transactions of Nonferrous Metals Society of China, 2003, 13(4): 750−754.

[24] HUANG L P, CHEN K H, LI S, SONG M. Influence of high-temperature pre-precipitation on local corrosion behaviors of Al−Zn−Mg alloy [J]. Scripta Materialia, 2007, 56(4): 305−308.

[25] LI Hui-zhong, YAO San-cheng, LIANG Xiao-peng, CHEN Yong-hui, LIU Cha, HUANG Lan. Grain boundary pre-precipitation and its contribution to enhancement of corrosion resistance of Al−Zn−Mg alloy [J]. Transactions of Nonferrous Metals Society of China, 2016, 26(10): 2523−2531.

[26] DENG Yun-Lai, WAN Li, ZHANG Yong, ZHANG Xin-ming. Evolution of microstructures and textures of 7050 Al alloy hot-rolled plate during staged solution heat-treatments [J]. Journal of Alloys and Compounds, 2010, 498(1): 88−94.

[27] XU D K, ROMETSCH P A, BIRBILIS N. Improved solution treatment for an as-rolled Al−Zn−Mg−Cu alloy. Part II: Microstructure and mechanical properties [J]. Materials Science and Engineering A, 2012, 534: 244−252.

[28] YANG X B, CHEN J H, LIU J Z, LIU P, QIN F, CHENG Y L, WU C L. Spherical constituent particles formed by a multistage solution treatment in Al−Zn−Mg−Cu alloys [J]. Materials Characterization, 2013, 83: 79−88.

[29] GUO Ran, ZHANG Cun-sheng, LIU Ming-fu, ZHANG Zhao-gang, CHEN Liang, ZHAO Guo-qun. Influence of isothermal and non-isothermal aging treatments on microstructure and properties of Al−Zn−Mg alloy helical profile [J]. Materials Characterization, 2020, 169: 110613.

[30] LI Nian-kui, CUI Jian-zhong. Microstructural evolution of high strength 7B04 ingot during homogenization treatment [J]. Transactions of Nonferrous Metals Society of China, 2008, 18(4): 769−773.

[31] LIU Man-ping, WU Zhen-jie, YANG Rui, WEI Jiang-tao, YU Ying-da, SKARET P C, ROVEN H J. DSC analyses of

static and dynamic precipitation of an Al−Mg−Si−Cu aluminum alloy [J]. Progress in Natural Science: Materials International, 2015, 25(2): 153−158.

[32] WANG Tao, YIN Zhi-min, SUN Qiang. Effect of homogenization treatment on microstructure and hot workability of high strength 7B04 aluminium alloy [J]. Transactions of Nonferrous Metals Society of China, 2007, 17(2): 335−339.

[33] XU D K, ROMETSCH P A, BIRBILIS N. Improved solution treatment for an as-rolled Al−Zn−Mg−Cu alloy. Part I: Characterisation of constituent particles and overheating [J]. Materials Science and Engineering A, 2012, 534: 234−243.

[34] TRIPATHI A, SAMAJDAR I, NIE J F, TEWARI A. Study of

grain structure evolution during annealing of a twin-roll-cast Mg alloy [J]. Materials Characterization, 2016, 114: 157−165.

[35] HUANG Ke, MARTHINSEN K, ZHAO Qing-long, LOGÉ R E. The double-edge effect of second-phase particles on the recrystallization behaviour and associated mechanical properties of metallic materials [J]. Progress in Materials Science, 2018, 92: 284−359.

[36] XU D K, BIRBILIS N, LASHANSKY D, ROMETSCH P A, MUDDLE B C. Effect of solution treatment on the corrosion behaviour of aluminium alloy AA7150: Optimisation for corrosion resistance [J]. Corrosion Science, 2010, 53(1): 217−225.

单级和多级固溶处理对 7055 铝合金螺旋面型材显微组织和性能的影响

张存生，张兆刚，刘明甫，鲍恩成，陈 良，赵国群

山东大学 材料液固结构演变与加工教育部重点实验室，济南 250061

摘 要：采用差示扫描量热法(DSC)、光学显微镜(OM)、扫描电子显微镜(SEM)、电子背散射衍射(EBSD)和透射电子显微镜(TEM)方法，研究单级固溶处理(SST)、强化固溶处理(EST)、高温预析出(HTPP)和多级固溶处理(MST)对挤压态 7055 铝合金螺旋面型材的显微组织、力学性能和耐蚀性的影响。研究发现，与传统的 SST 相比，EST 和 MST 能促进第二相颗粒的溶解，而 HTPP 和 MST 处理后合金的晶间相呈明显的不连续分布状态。不同固溶制度处理后合金的主要织构类型和织构强度存在明显差异。HTPP 可以通过调节晶间相的分布提高合金的耐蚀性，但其力学性能严重削弱。MST 可以使合金获得良好的耐蚀性，而并未造成明显的强度损失。结果表明：MST 为 7055 铝合金较为理想的固溶处理方式。

关键词：7055 铝合金；挤压型材；固溶处理；力学性能；耐腐蚀性

(Edited by Xiang-qun LI)